

Resistance Spot Welds of 304I Austenitic Stainless Steel, Part 1: Fundamental, Simulation, Weld Growth, Tensile Strength And Failure Mode Analysis

Nachimani Charde

Department of Mechanical Engineering, Faculty of Engineering, University of Malaya, 50603 Kuala Lumpur, Malaysia Email: nachicharde@yahoo.com

ABSTRACT

Austenitic stainless steel (ASS) is a very common material that is used in many industries today. A suitable joining method should be of low cost; reliable and long life. In such a situation, the industries may prefer to use the resistance spot welding (RSW) for such ASS sheet. The weld quality of an RSW joint is usually considered by nugget size, which relies on the welding parameters. This paper analyzes the weld nuggets' characteristics of 304L austenitic stainless steel with relevant to its basic welding parameters (current, weld time and force). The entire experiment is carried out by varying the welding current and welding time at first attempt and the welding current and electrode force at second attempt. The increment of current and weld time has resulted in a proportional increment of nugget diameters; whereas the force increment has resulted in a reduction of nugget diameters. These results have been relatively compared with simulation results for the proper weld region identification. Eventually, the welded joints were characterized by tensile shear test, macro graph and elongation measurement to relate the changes that happened due to the variations of welding parameters.

Keywords: Welding Simulation, Stainless steel welding, Tensile simulation, Elongation simulation.

1.0 INTRODUCTION

Joining the metal sheets together is easily accomplished by using resistance spot welding technology, nowadays. This welding process basically uses two copper electrodes to compress the sheets together and supplies a huge amount of current which flows through the metal sheets that are placed between electrodes [1]. The flow of current against the series of resistances causes heat development between the metal sheets and gradually melts the concerned areas [2]. Mathematically, the heat generation is given by $Q = kI^2Rt$; where I^2 is the welding current, R is the total resistance, t is the time and k is the heat loss factor [3]. The most varying parameter during the welding process is the total resistance ($R = R_1 + R_2 + R_3 + R_4 + R_5$) of the joining area, as it consists of the

upper electrode surface to the upper metal sheet surface resistance (R_1), the upper metal sheet's bulk resistance (R_2), the resistance between sheet to sheet surfaces (R_3), the lower metal sheet's bulk resistance (R_4) and the lower metal sheet surface to lower electrode surface resistance (R_5) shown in **Fig. 1**. When the current flow is fully stopped, the melted area would be undergoing cold work [4]. The melted and solidified areas of base metals are thereafter called as weld nugget and it consists of major three zones; firstly the fusion zone (FZ), secondly heat affected zone (HAZ) and thirdly the base metals (BM). Thus, the proper joints between the sheets are usually formed at the fusion zone due to complete fusion and solidification processes [5]. The melting capability is dependant of thermal conductivity and electrical resistivity of

stainless steel; as the physical properties varies from one material to another [6]. The areas adjacent to fusion zone are the heat affected zone at which the partial melt does exist and it happens due to the thermal conductivity of base metals. This thermal conductivity allows the heat to flow along the base metal but gradually reduces the amount as it flows away. The portions that the thermal conductivity does not alter the chemical properties are remained as base metals [7]. As the weld nugget starts to grow, the process parameters such as welding current, welding time, electrode force and electrode tips diameter play an important roles during the process. These four common parameters that enable to weld nugget growth, also control to produce sound welds leading to development of stiffness of metal joints if properly aligned. In this experiment, the current, weld time and force are varied to characterize the weld nugget growth while electrode tip is kept constant.

2.0 EXPERIMENTATION

Some mathematical considerations are carried out to ensure that the welding process meets the basic criterion [8]. Initially the electrode diameter is calculated according to the Miller's guide, as follows. The electrode tip diameter is given by, D_e (mm) = 2.54 mm + 2t; where t is the thickness of one side of metal sheet in mille meter. Hence the diameter of tip in this research work is calculated as D_e (mm) = 2.54 mm + 2 (1 mm) = 4.54 mm; for 1 mm thickness of sheets. A pair of truncated electrode tip of 5 mm diameter is selected from RWMA's class two (copper and chromium) category. The resistance of the stainless steel pair is calculated as, $R = \rho l/A$; Let ρ be the resistivity of stainless steel ($6.89 \times 10^{-7} \Omega m$), l be the length of the path that the current flows regardless of inter-surface gap ($l = 1 \times 10^{-3} + 1 \times 10^{-3} = 2$ mm) and A be the area of the path that the current flows ($A = \pi r^2 = (3.14)(2.5 \times 10^{-3})^2 = 19.634 \mu m^2$). So, $R = \rho l/A = (6.89 \times 10^{-7}) (2 \times 10^{-3}) / (19.634 \times 10^{-6}) = 70.18 \mu \Omega$. Let's calculate the range of resistances that can be welded using 75 kVA spot welders for 1mm thickness. The nominal power of the spot welder is the 75 kVA and the secondary current is 25 kA maximum. Now the secondary voltage is calculated by $V_s = V_p I_p / I_s(\max) = 75000 / 25000 = 3V$ (max). So when the current is as low as 1 A, the resistance $R = V_s / I_s = 3/1 = 3\Omega$ (max); but when the current is as high as 25 kA, the resistance $R = V_s / I_s = 3/25 \times 10^3 = 120 \mu \Omega$ (min). However these calculated values ($P = I^2 R$) may vary practically ($Q = I^2 R t$) as the time factor 't' is introduced in the heating duration. There are other factors such as voltage drops in the winding, magnetic losses, core losses, copper losses and extras may also cause

variation in practical results. The stainless steels' samples are prepared as 200 mm long by 25 mm wide from 1 mm thickness sheets. The chemical elements that found on this sample sheets are: C = 0.048, Cr = 18.12, Ni = 8.11, Mn = 1.166, Si = 0.501, S = 0.006, N = 0.053 and P = 0.030. It has original hardness level of 81.7 HRB; elongation level of 40% from 50 mm long; and tensile strength of 515 MPa. The stainless steel sheets are welded at the centre of 60 mm of overlap as shown in Fig. 1.

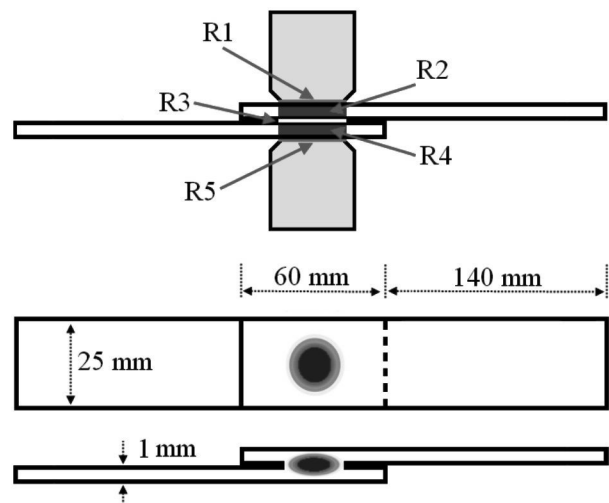


Fig. 1 : Test Sample

The test samples are initially placed on the top of lower electrode's tip of the spot welder (Table 1) as overlapping of 60 mm on each other and then the initiating pedal is pressed. The welding process is started right after the squeezing cycles end. Thus, once the squeezing force is reached to its present-preset value, the welding current is delivered in accordance with. Thereafter the electrode pressing mechanism (pneumatic based) consumes some time for cold work and eventually returned to the home position of upper electrode. In order to get a proper weld nugget, the process controlling parameters (current, weld time and force) have to be selected and set before the welding process starts [9]. So the welding lobe is initially developed for welding current and welding time and later for welding current and electrode pressing force.

Table 1 : Specification of JPC 75kVA spot welder

Description	Amount
Rated capacity	75 kVA
Rated primary voltage	240 V
Rated secondary voltage	1 ~ 3 V
Rated frequency	50 Hz
Rated secondary current (max)	25 000 A
Tip diameter	16 mm (max)
Maximum electrode force	1000 Kg
Upper electrode stroke	10 ~ 60 mm
Quantity of cooling water	12.7 l/min
Net weight (approx.)	380 Kg

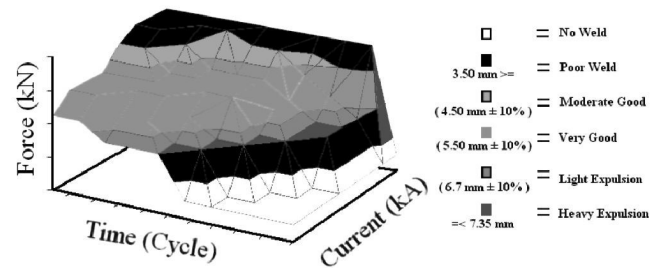


Fig. 3 : A 3D view of welding lobe for 1 mm austenitic stainless steel

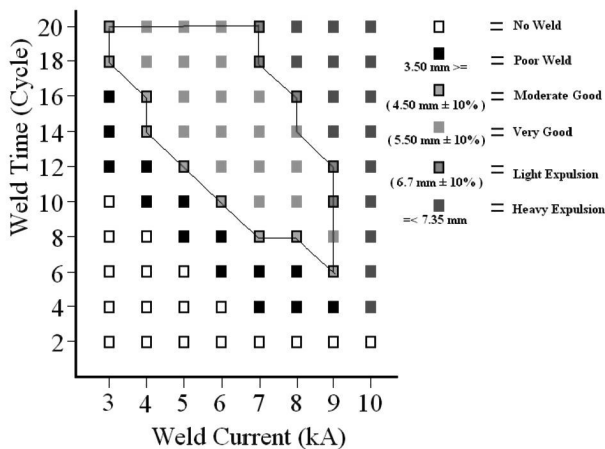


Fig. 2(a) : Welding lobe for welding current versus welding time

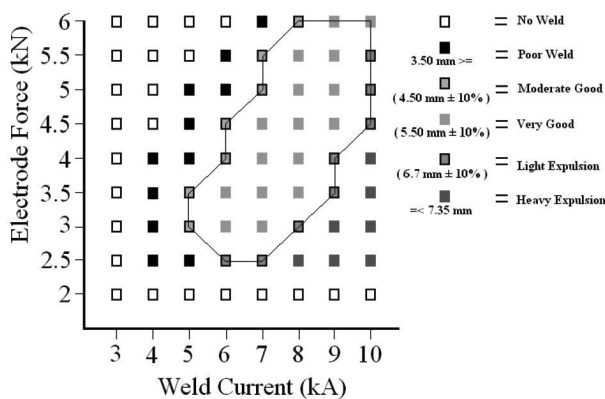


Fig. 2(b) : Welding lobe for welding current versus electrode pressing force

Fig. 2(a) shows the welding lobe curve or window of operation of welding current against the welding time for 1 mm metal sheets after underwent several welding processes on sample sheets. The lobe boundary is indicated by continuous black colour lines delineates all acceptable welding regions. The coloured symbols represent the quality of welds that produced. So the conditions that did not produce any weld are indicated by white boxes. The grey coloured boxes with black borders represent moderate to good welds; the fully green boxes represent very good welds; the light-red coloured boxes bordered in black represent welds for which light expulsion occurred; the red boxes represent heavy expulsion and the black boxes represent poor weld joints. Similarly, the **Fig. 2(b)** was developed for various welding current against welding force. **Fig. 3** shows the 3D view of welding lobe for welding current, welding time and electrode force. A weld schedule is finally developed based on the welding lobe curves as shown in **Fig. 3** to avoid expulsion and also poor welding conditions because the scope of this paper is to investigate the weld growth in good working regions, only! So the entire welding processes are accomplished for three levels of welding current (6, 7, 8 kA); welding time (10, 15, 20 cycle) and electrode force (3, 4.5, 6 kN). Based on this simple computation, nine weld schedules are finalized (**Table 2**). During the welding process, seven pairs of specimens are welded for each weld schedule (critical diameter growth $D_{(mm)} \geq Kt^{0.5}$; $t = 1$ mm and $K = 4$). Among these welded pairs, five out of seven are used for tensile test and the corresponding average value is considered for that particular weld schedule. One pair of specimen is used for hardness test and the final one pair of specimen is used for metallurgical test (Part 2 discusses the hardness and metallurgical changes).

Table 2 : Weld schedule

Both		Welding Current and Weld Time			Welding Current and Electrode Force	
Sample No.	Weld Schedule	Current (kA)	Time (cycle)	Force (kN)	Time (cycle)	Force (kN)
1-7	1	6	10	3	10	3
8-14	2	7	10	3	10	3
15-21	3	8	10	3	10	3
22-28	4	6	15	3	10	4.5
29-35	5	7	15	3	10	4.5
36-42	6	8	15	3	10	4.5
43-49	7	6	20	3	10	6
50-56	8	7	20	3	10	6
57-63	9	8	20	3	10	6

3.0 RESULTS AND DISCUSSION

3.1 Simulation of Stainless Steel Spot Weld

Simulating the welding process of stainless steel sheets were conducted for the 1mm thickness using Visual Basic as shown in (Fig. 4b, c, d and e)). The simulation formulas and analysis set up are all avoided as it involves complex formulation and also discussion. So only the results are presented here for simplicity. The simulation results show significant behaviour of stainless steels when it is welded according to the weld schedule conditions as listed in Table 2. The thermal conductivity coefficient rate is lower in stainless steel as compared to other materials (For example: carbon steel) so the heat affected zone seems very shorter next to fusion zone in stainless steel [10]. However, the diameter growth seemed to be reasonably acceptable as compared to the real weld nuggets as shown in Figs. 6, 7, 8, and 9.

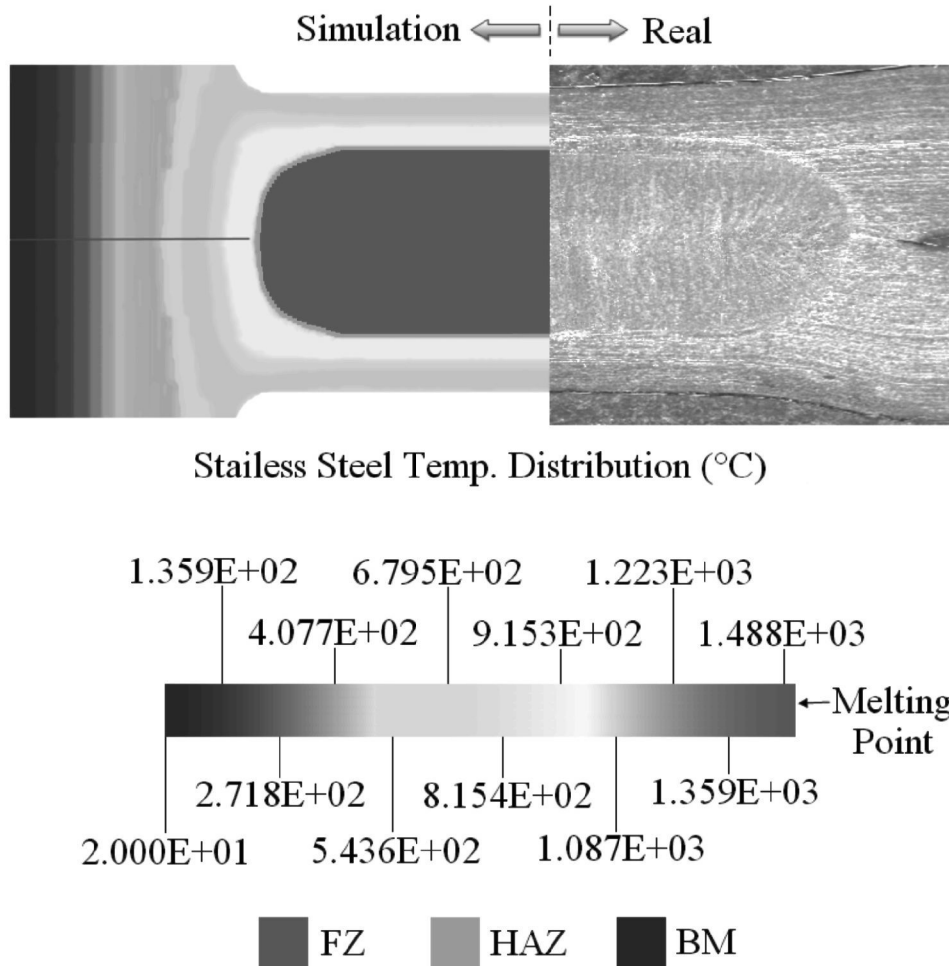


Fig. 4(a) : A real and simulated macrograph for stainless steel welds regions.

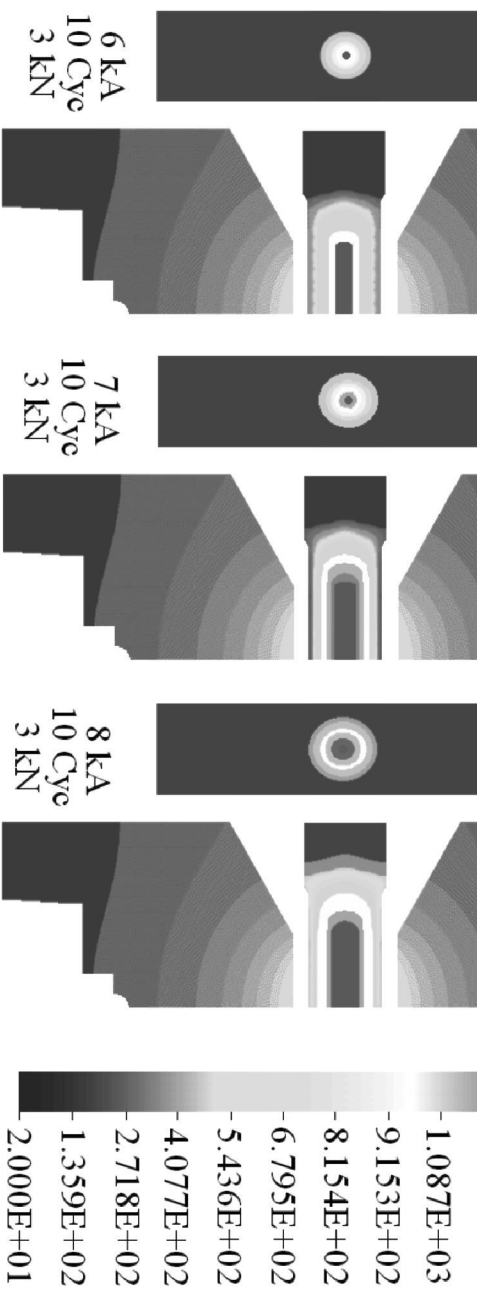


Fig. 4(b) : Simulation for welding current increment (Welding current and welding time)

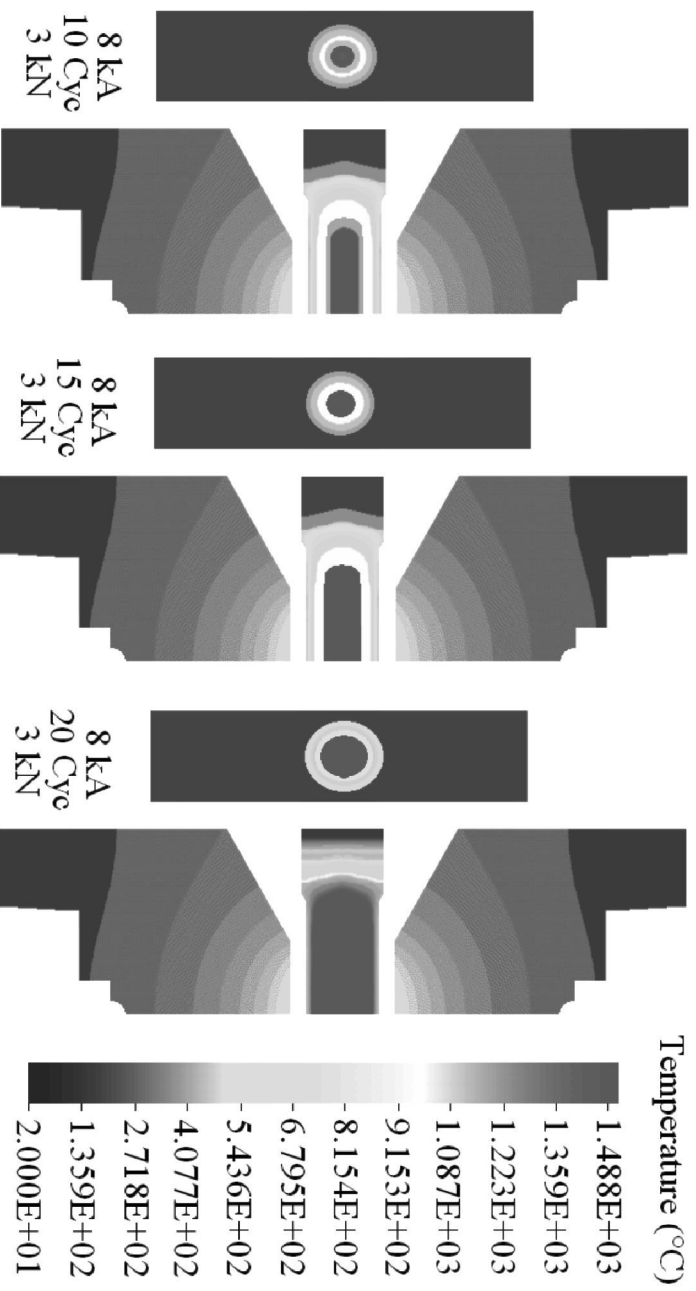


Fig. 4(c) : Simulation for welding time increment (Welding current and welding time)

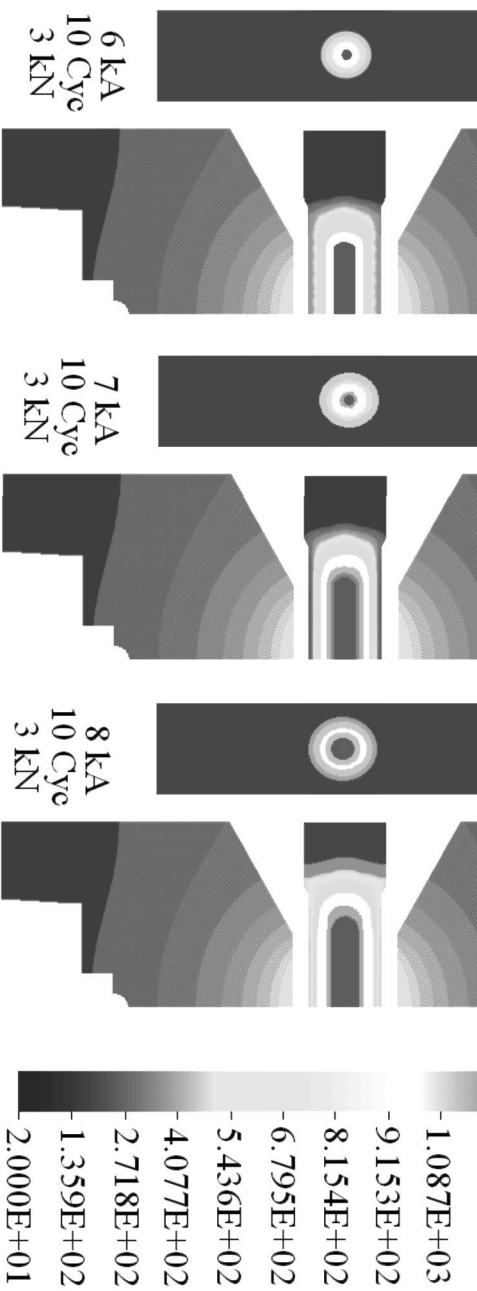


Fig. 4(d) : Simulation for welding current increment (Welding current and electrode force)

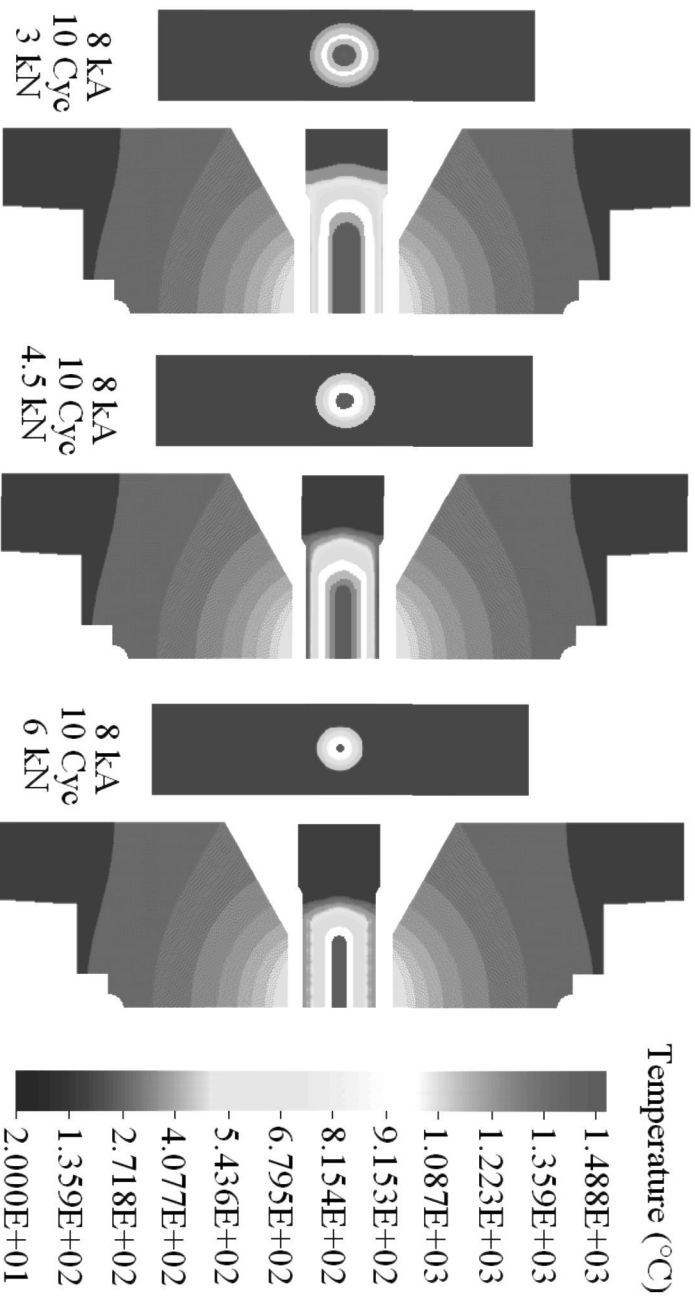


Fig. 4(e) : Simulation for electrode force increment (Welding current and electrode force)

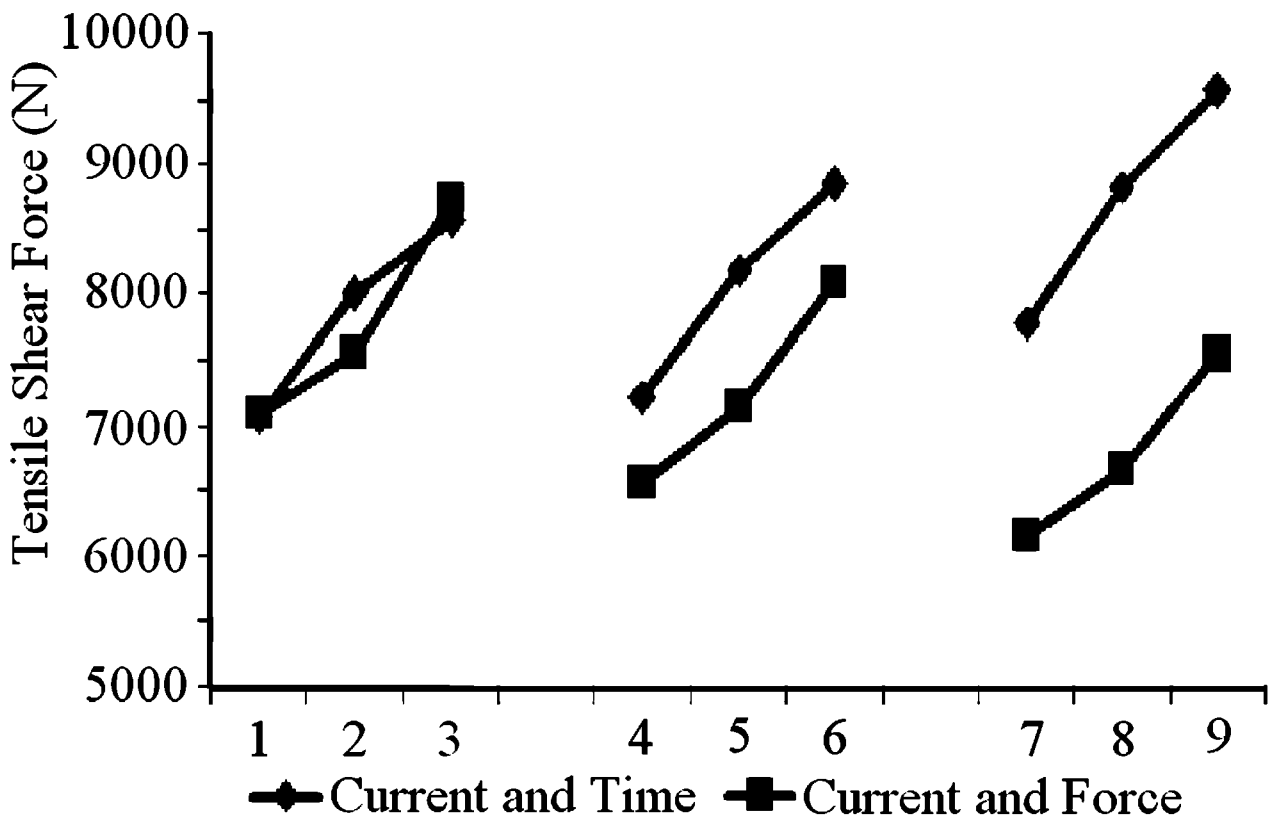


Fig. 5 : Tensile shear test results

3.2 Tensile Shear Strength

Assessing the welded samples under the tensile shear test (Fig. 5) is a common practice in determining the strengths [11]. Similar test has been conducted to finalize the ultimate tensile strength (UTS) for both category of experiment (the welding current against welding time variations; and the welding current against the electrode force variations) [12]. The crosshead speed is maintained at 70 mm/min. The ultimate tensile strength (UTS) is taken as the maximum weld strength after which the welded joints have fractured. The average strength values from the five samples are taken as the equivalent strength of that particular weld schedules [13]. As for the weld schedules from 1 to 2 and 2 to 3; the strength increment is noticed due to the increment of welding current from 6 kA (4.263 mm) to 7 kA (4.441 mm) and 7 kA (4.441 mm) to 8 kA (4.692 mm), respectively. The similar increments are also noticed for the following weld schedules of 4, 5 and 6 as well as 7, 8, and 9. This obviously shows that increase in current has caused increase in strength due to the increase of weld diameter, accordingly. Likewise, the current increment is found in both sets of attempts (Fig. 8). When the current and

weld time incremental set is considered: the weld time has also increased the tensile strength as it basically increases the diameters from weld schedule 1 (4.263 mm) to 4 (4.915 mm) and further increase from 4 (4.915 mm) to 7 (5.328 mm) as well (Fig. 6). This fulfils the Joule's law of heat dissipation in metals. By increasing either welding current or welding time, the heat supplied at the electrode tip is also proportionally increased and therefore the corresponding diameters increments are obtained (Fig. 6). However when the welding current and electrode pressing force incremental set is considered: the electrode force increment has caused strength reduction due to the drop of heat. For an example, when the force increments from 3 kN (4.681 mm) to 4.5 kN (3.702 mm) and 4.5 kN (3.702 mm) to 6 kn (3.026 mm) are considered; the tensile strength seemed to be reduced because the resistive components are reduced in the heating process which is another proportional coefficient of heat formula ($Q=I^2Rt$). Thus, the resistance is reduced by producing high electrode pressing force as it does changes in length (l) which is also another proportional coefficient of resistive equation. The bulk resistance of a single sheet is calculated from resistive formula;

such as $R = \rho l / A$; where ρ is the resistivity ($6.89 \times 10^{-7} \Omega \cdot m$); l is the length (1 mm for single sheet) and A is the contact area ($19.63 \mu m^2$) of electrode tip. The electrode tips are not changed at all so that the resistance is mainly affected due to changes in bulk resistance during squeezing as well as the contact resistances [14]. Obviously, **Fig. 6** shows the drop of diameters when increase of force is concerned in this experiment.

3.3 Electrode Indentation

Identifying the root cause for the indentation of a weld nugget is another important factor in the spot welding analysis although it is very obvious that the electrode pressing force is the root cause for any indentation at the welded areas (**Fig. 7**). These pressing forces may create a circumstance to splash out the molten metal from the concerned areas when the molten areas grow beyond its limits or due to an unclean electrode tip with excessive pressing forces. What so ever, the indentations are somehow measured for the variation of basic welding parameters.

When all of the process controlling parameters (welding current, welding time and electrode pressing force) are increased; the indentation goes deeper on both sides of base metals as how theoretically predicted before. In most cases, the indentations are rather deeper on upper electrode side because upper side is always pressed by pneumatic cylinder and also exposed to direct impact during squeezing cycles. Further to these pressing forces issues, the electrically generated forging forces do exist due to the huge AC current flow from upper electrode through base metals to lower electrode and vice versa. **Fig. 8** shows the overall indentation values of welded areas for the welding current, welding time and electrode pressing force variations.

3.4 Failure Modes

Having considered the failure modes of tensile shear test; the stress-strain relationship is simulated using Visual Basic as to understand the weld failures graphically. The general formula for the uniaxial force with respect to phase angle is given by, $F(\theta) = F(\max) \cdot \cos(\theta)$; where 'F(max)' stands for the tensile pulling force in Newton; and the ' θ ' stands for phase angle of tensile-broken samples as it varies from 0 to 90° practically for interfacial (IF), partial (PF) and full-button pullout (TF) failures. So the uniaxial stress that existed on weld bead during tensile test is computed as follows: $\text{Stress} (\tau) = F(\max) \cdot \cos(\theta) / \tau \cdot r^2(\text{weld}) \cdot H(\text{weld})$; where $r(\text{weld})$ is the weld radius (meter) obtained from **Fig. 6** and $H(\text{weld})$ is the weld height (meter) obtained from real weld. This equation is an easy way to

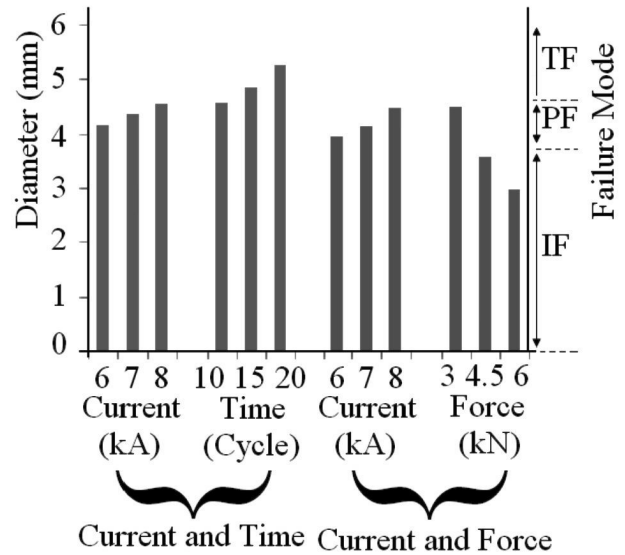


Fig. 6 : Diameter of Weld Nuggets and Failure Modes

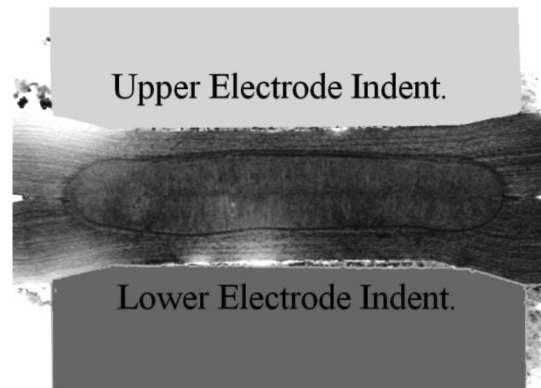


Fig. 7 : Upper and lower Indentation of welded area

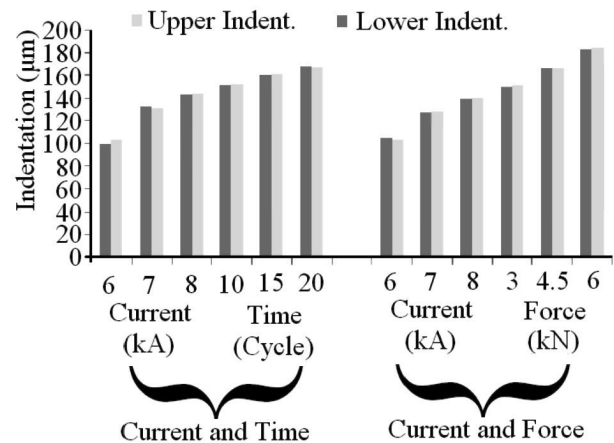


Fig. 8 : Indentation of the welded areas (various parameters variations)

compute the stress intensity for the cylindrical weld bead but the areas may vary for different weld joints practically. Theoretically there are many ways to compute the equation for tensile shear strength but is purely complex and vary in reality [15]. As such the primary intention on this type of simulative works is to visualize the strain distributions on sample sheets rather than predicting precise-stress intensity at the welded regions [16]. Thereby, the broken samples are measured for its tilt angle (θ) as well as the radius and the height of weld beads. **Fig. 9** shows a simulation work for the austenitic stainless steel of 1mm thickness sheets with practical measurements. They are specifically simulated with real measurements from failures: (a) IF with $\approx 15^\circ$; (b) IF with $\approx 30^\circ$; (c) IF with $\approx 45^\circ$; (d) PF with $\approx 30^\circ$; and (e) TF with $\approx 30^\circ$ of tilt angle.

Practically a poor weld has interfacial fracture (IF) and the shear-force seemed to be falling between 6 to 7 kN for 1 mm thickness. A moderate-good weld has tear from one side of base metal (PF) and; the shear force falls between 7 to 8 kN in this experiment. Likewise a good weld has better bounds between sheets and therefore it requires higher shear force to break the joints (8 to 10 kN; in this case). Often it tears from both sides and button pullout (TF) of the base metals as the break does not occur at the welded area but rather at the heat affected areas [17]. Ever since the heat affected areas alters itself in hardness (slightly higher than base metals); both sides hold the welded areas firmly during tensile pulling to an extent where the tear trail enters the base metal regions and then breaks [18]. **Fig. 10(a)** shows the failure modes with indicating regions of IF, PF and TF regions while **Fig. 10(b, c and d)** are showing the physical breaks respectively.

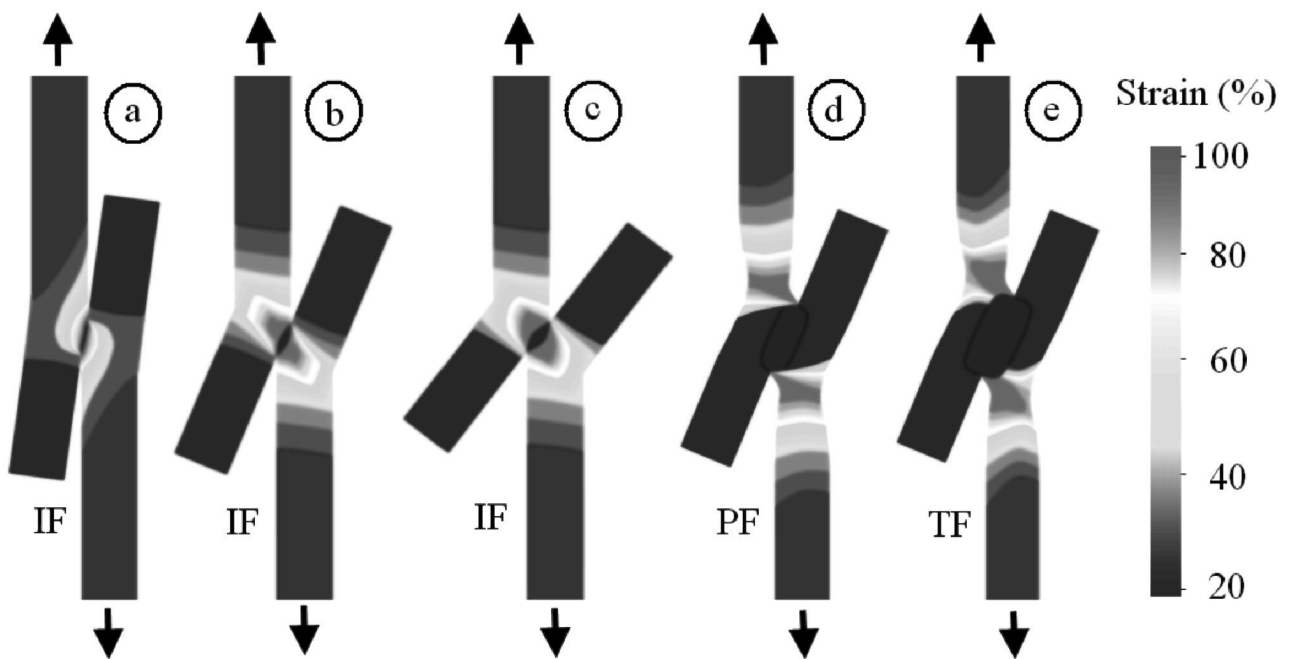


Fig. 9 : Tensile shear test (strain distribution)

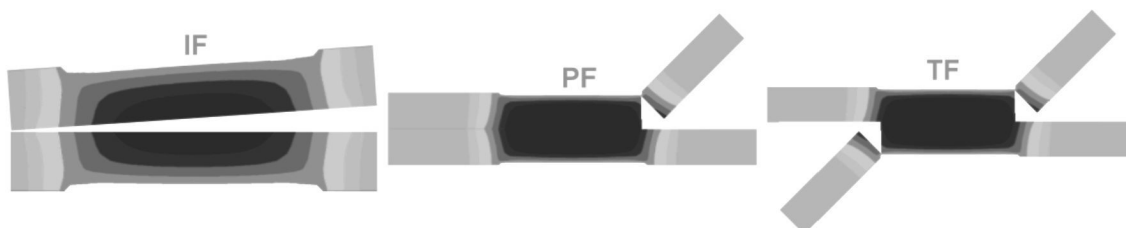


Fig. 10(a). Failure modes

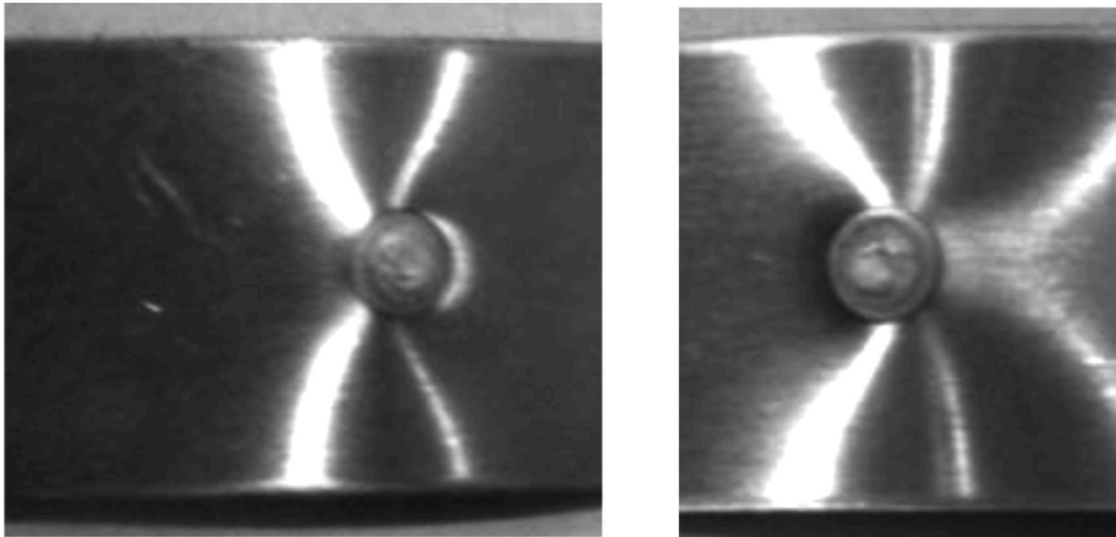


Fig. 10(b) : Interfacial failures (IF)

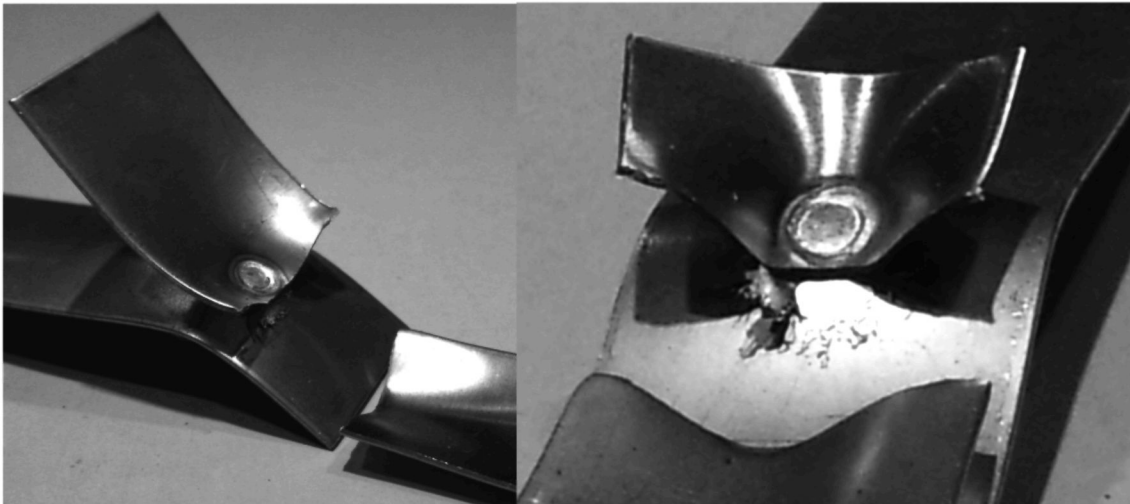


Fig. 10(c) : Tear from one side (PF) failures

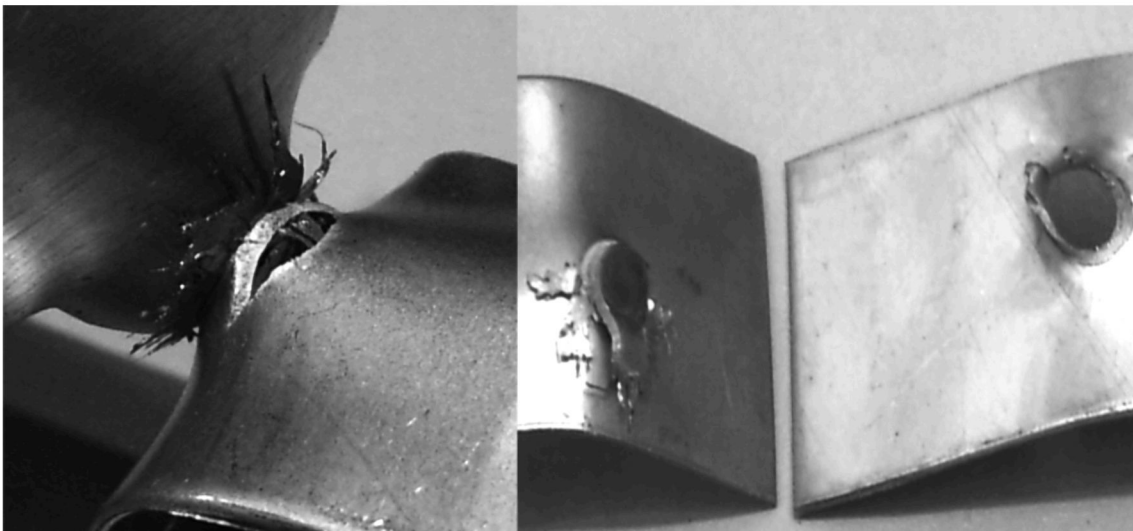


Fig. 10(d) : Tear from either side or button pullout (TF) failures

3.5 Failure Modes Elongation

Elongation that subjected to the tensile shear test is another factor to understand the failure modes as it shows the heavily strained regions in addition to the deformed surfaces, physically. A post failure crack propagation mode is executed rather than just seeing at the normal failure crack mode during tensile test. By doing so, the PF and TF modes can be relatively differentiated [19,20]. The tear from one side (PF) is shown in **Fig. 11(a)** and the tear from both sides is shown in **Fig. 11(b)** (TF) [21]. They are easily seen from their elongation. Although both, the PF and TF consumed more forces as compared to IF, the conventional way does not separate them for their individual characteristics. TF is better than PF and both are better than IF. See **Fig. 11 (d and e)**; as the poor interfacial failures (IF) have minimum elongation as compared to PF and TF. All the distinct separation can be physically seen through the **figures from 11(a) to figure (e)**.

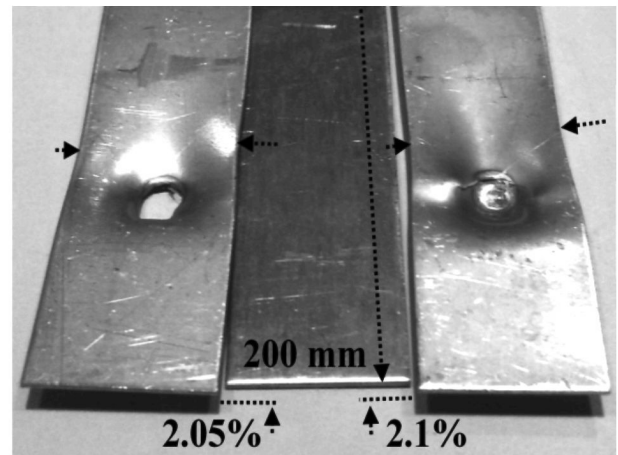


Fig.11(c) : TF mode (button pullout)

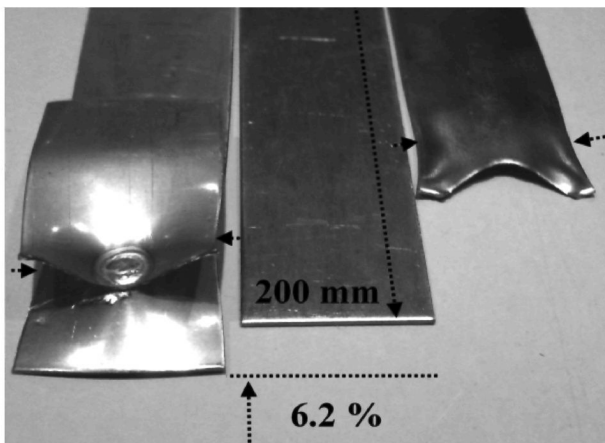


Fig. 11(a) : PF mode

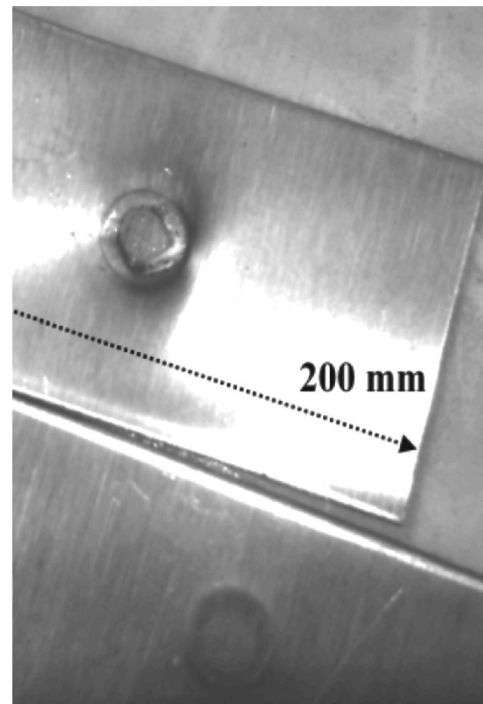


Fig. 11(d) : IF mode (poor fracture)

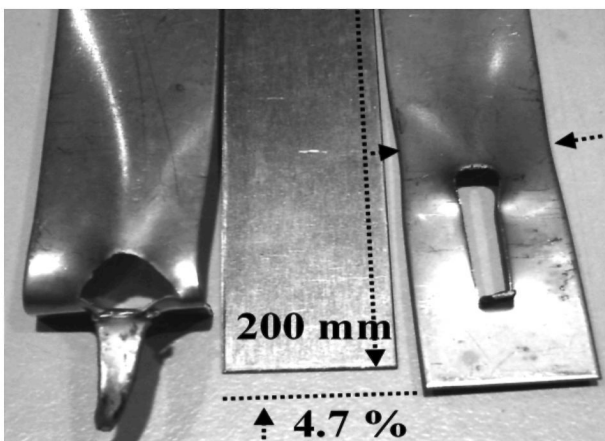


Fig. 11(b) : TF mode (both side fracture)

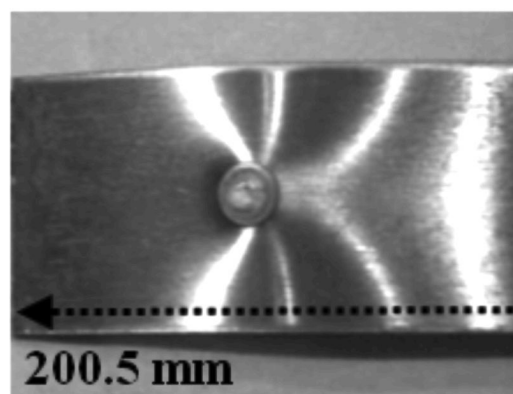


Fig. 11(e) : IF mode (better fracture)

So the elongation in term of percentage is usually measured as follows: $E (\%) = [\text{Length}(\text{after broken}) - \text{Length}(\text{original}) / \text{Length}(\text{original})] \times 100$; where Length(after broken) is the length that changed after underwent the tensile test and

Length(original) is the original length of welded sheets. The descending order of % Elongation with the fracture mode could be represented as PF,TF (both side), TF (button pull out)and IF.

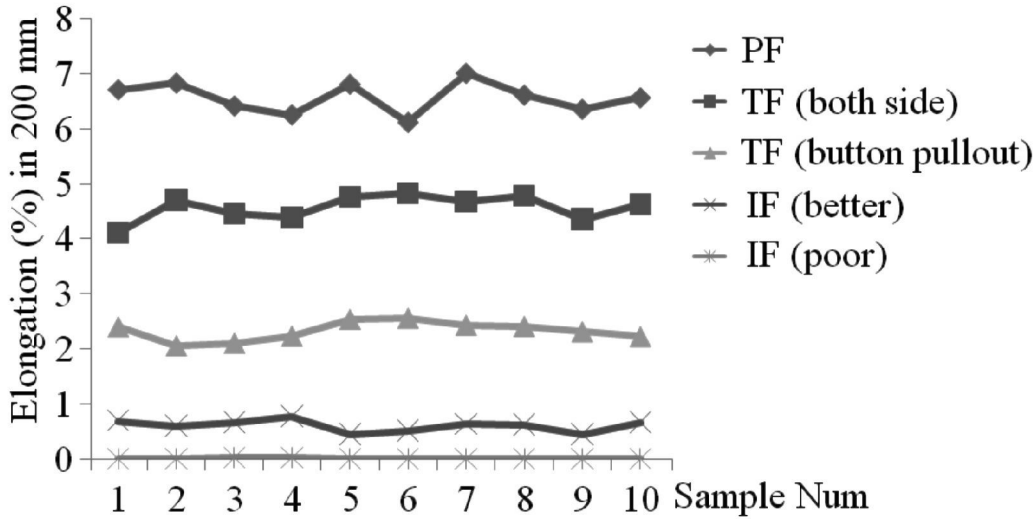


Fig. 11(f) : Elongation in % for various failure modes

CONCLUSION

This paper looks into the spot weld growth on 304L austenitic stainless steel with 1 mm thickness sheets and it concludes that:-

1. Welding lobe is equally spaced for 6, 7, and 8 kA; 10, 15 and 20 Cycle; 3, 4.5, and 6 kN of parametric alignments to characterize the proper working regions.
2. Simulation for the welding lobe values show that the welding time and welding current are proportional to heat while electrode force is inversely proportional to heat within the welding lobe.
3. Increase in welding current and welding time within the weld lobe have resulted increment in diameter of weld nuggets and therefore the increment of tensile shear force is noticed.
4. Increase in electrode forces have resulted decrement in diameter of weld nuggets and therefore the decrement of tensile shear force is also noticed.
5. The micro indentation of electrodes has resulted proportional relationship for all the changes in basic parameters (Welding current, welding time and electrode force).

6. Simulation of the tensile shear test is carried out to visualize the strain intensity during tensile test. It shows multiple strain distributive patterns for different failure modes based on its tilt angles.
7. The post crack propagation modes are seen during tensile test and poor weld joint shows interfacial fracture (IF); a better weld produces tear form one side (TF); and very good weld shows button pullout or tear from both sides (PF) when pull to break mode is actuated.
8. The PF mode has resulted high % elongation as compared to other two failure modes i.e. TF and IF.

ACKNOWLEDGEMENTS

I would like to thank Ministry of Science, Technology and Innovation of Malaysia (MOSTI) for its financial support throughout the experimentations. This research outcome is part of Nachimani's PhD research work.

REFERENCES

1. Aravinthan A. and Nachimani C. 2011. Analysis of spot weld growth on mild and stainless steel. *Welding Journal*, August: 143-147.
2. Nachimani C. 2012a. Effect of spot welding variables on nugget size and bond strength of 304 austenitic stainless steel (2 mm). *Australasian Welding Journal*, Vol 57:1-7.
3. Dursun O. 2008. An effect of weld current and weld atmosphere on the resistance spot weld ability of 304L austenitic stainless steel. *Materials and Design*, 29: 597-603.
4. Shamsul JB and Hisyam MM. 2007. Study of spot welding of austenitic stainless steel type 304 *Journal of Applied Sciences Research* 3(11), 1494-99.
5. Yang Y and Sung G. 2011. Effect of resistance spot welding parameters on the austenitic stainless steel 304 grade by using 23 factorial designs. *Advanced Materials Research*, 216: 666-70.
6. Fukumoto S. 2008. Small scale resistance spot welding of austenitic stainless steels. *Materials Science and Engineering A*, 492: 243-49.
7. Jamasri S. 2011. Corrosion fatigue behavior of RSW dissimilar metal welds between carbon steel and austenitic stainless steel with different thickness. *Procedia Engineering*, 10: 649-54.
8. Oscar M. 2009. Quality prediction of resistance spot welding joints of 304 austenitic stainless steel. *Materials and Design*, 30: 68-77.
9. Cha BW and Na SJ. 2003. A study on the relationship between welding conditions and residual stress of resistance spot welded 304-type stainless steels. *Journal of Manufacturing Systems*, vol 223: 344-53.
10. Feramuz K. 2009. The effect of process parameter on the properties of spot welded cold deformed AISI304 grade austenitic stainless steel. *Journal of Materials Processing Technology*, 209: 4011-19.
11. Nachimani C. 2012b. Spot weld growth on 304L austenitic stainless steel for equal and unequal thicknesses. *Caspian Journal of Applied Sciences Research* 1(11), 79-87.
12. Triyono. 2012. Fatigue behavior of resistance spot-welded unequal sheet thickness austenitic stainless steel. *Modern Applied Science*, 45: 345-55.
13. Pouranvari M. 2011a. Effect of welding current on the mechanical response of resistance spot welds of unequal thickness steel sheets in tensile-shear loading condition. *International Journal of Multidisciplinary Sciences and Engineering* 2: 44-52.
14. Wei Lee. 2012. The influences of nugget diameter on the mechanical properties and the failure mode of resistance spot-welded meta stable austenitic stainless steel. *Materials and Design*, 33: 292-99.
15. Lee WS. 2004b. Deformation and failure response of 304L stainless steel SMAW joint under dynamic shear loading. *Material Science Engineering*, 381: 206-15.
16. Pouranvari M. 2008b. Prediction of failure mode in AISI 304 resistance spot welds. *Journal-Association of Metallurgical Engineers of Serbia* 46 1-6.
17. Nordberg H. 2005. Fatigue properties of stainless steel lap joints. *SAE Transactions: Journal of Materials & Manufacturing* 114, 675s-90s.
18. Kent P. 2000. Comparison of peel bond and shear tensile test methods for needle punched geo synthetic clay liners. *Geotextiles and Geomembranes*, 18: 203-14.
19. Lee WS. 2007a. Effects of strain rate and welding current mode on micro structural properties of SUS 304L PAW welds. *Journal of Material Processing Technology*, 183: 183-93.
20. Pilar DT and Oruk TT. 2011. Use of EPR test to study the degree of sensitization in resistance spot welding joints of AISI 304 austenitic stainless steel. *Corrosion Science* 53, 1563-70.
21. Pouranvari M and Marashib SPH. 2010. Failure mode transition in AHSS resistance spot welds, Part I: Controlling factors. *Materials Science and Engineering A* 528, 8337- 43.